Third International Conference on Sustainable Construction Materials and Technologies http://www.claisse.info/Proceedings.htm

Investigation of Corrosion Rate in Reinforced Concrete Structure

Shinichi Miyazato[1]

[1]*Kanazawa Institute of Technology, Japan*

ABSTRACT

Some research has been conducted on the chloride ingress. However, there is little research about the steel corrosion rate in concrete. Therefore, the steel corrosion rates in existing structures were investigated in this study. First, the investigation method for the steel corrosion rate in concrete is explained. The corrosion rate, considering both macrocell and microcell, is analyzed using the measured potentials, polarization resistances, and concrete resistivities. All of these input values can be measured by a nondestructive testing method. Second, this paper explains how this method was used to investigate the corrosion rate in an existing concrete beam that had been repaired. This made it possible to quantitatively monitor the steel corrosion rates in the concrete. Moreover, it was confirmed that the corrosion rate at 10 a.m. and the average rate for a day were equivalent. This indicates that the annual average corrosion rate can be estimated by monitoring.

Keywords. Steel corrosion, Macrocell, Monitoring, Existing structure

INTRODUCTION

When concrete has a defect such as a crack or joint, the distribution of the oxygen, water, and chloride ions becomes nonuniform. As a result, macrocell corrosion is generated locally. On the other hand, microcell corrosion progresses uniformly throughout the entire member. Generally, the macrocell corrosion rate is higher than the microcell corrosion rate (Otsuki et al. 2000; Miyazato and Otsuki 2010). Therefore, it is necessary to evaluate not only the microcell corrosion rate but also the macrocell corrosion rate. However, only the microcell corrosion rate in reinforced concrete structures has been evaluated because no method exists for measuring the macrocell corrosion rate.

Based on the background, the objectives of this study are as follows. 1) An electric circuit model that estimates the macrocell corrosion rate is proposed. 2) Through experiments using a specimen with bending cracks, the validity of the electric circuit model is quantitatively investigated. 3) The macrocell corrosion rate is monitored in an existing reinforced concrete beam with a repair. 4) A reasonable maintenance method is suggested based on the corrosion.

PROPOSITION OF ELECTRIC CIRCUIT MODEL

Assumption. A thin layer called an electric double layer exists on a steel surface. When this is replaced with an electric circuit, it can be considered as a parallel-connected resistance

and condenser. However, the condenser does not control the corrosion rate in the steady state, because the macrocell corrosion current in concrete flows in only one direction. Therefore, the condenser is not included in an electric circuit model. In addition, the transfer of electrons and ions between the anode and the cathode in concrete should be evaluated using the electrical resistivity of the concrete (concrete resistance).

Construction of Electric Circuit Model. An electric circuit model of a macrocell formed in reinforced concrete is shown in Figure 1. This circuit consists of the polarization resistance and electrical resistivity of the concrete. Both the polarization resistance and electrical resistivity of the concrete can be measured by a nondestructive test for an existing reinforced concrete structure. In addition, the potential, which can also be measured by a nondestructive test, is also substituted for the electric circuit model.

Herein, the current that flows between two randomly selected points is calculated using Ohm's law, as shown in Equation 1. In addition, based on Kirchhoff's law, the total current that flows from the adjoining points to the selected point becomes 0. For example, Equation 2 can be utilized for point 0 shown in Figure 2. Equation 1 is substituted into Equation 2. Then, an equation that corresponds with Equation 3 is derived for every point. Afterward, by converting all of the equations into simultaneous equations, the potential in the concrete is calculated in a medium analysis stage. Finally, the potentials of two adjoining points and the resistance between them are substituted into Equation 1, and the macrocell corrosion current that flows between the points is calculated.

$$I = \frac{V_j - V_k}{R} \tag{1}$$

$$\sum_n I_i = I_1 + I_2 + I_3 = 0 \tag{2}$$

$$\frac{V_1 - V_0}{R_1} + \frac{V_2 - V_0}{R_2} + \frac{V_3 - V_0}{R_3} = 0 \tag{3}$$

where I = current; V = potential; and R = resistance.

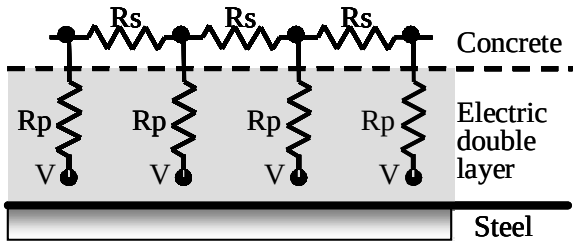

Rp : Polarization resistance,
Rs : Electrical resistivity of concrete,
V: Potential

Figure 1. Electric circuit model of macrocell formed in reinforced concrete

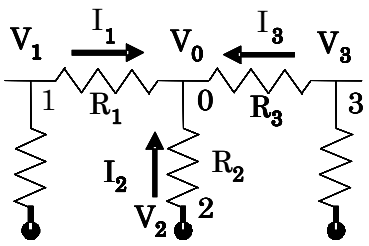

Figure 2. Current balance at selected point

EXPERIMENT WITH MORTAR SPECIMEN

Experimental Procedure. Table 1 lists the characteristics of the materials used. Ordinary Portland cement was used for the cement. A naphthalene-based high-range water-reducing agent was used for mortar with a 30% water cement ratio.

Table 1. Materials used

	Type	Characteristics
Cement	OPC	Density = 3.15 g/cm^3, Specific surface = 3.27 m^2/kg
Fine aggregate	Land sand	Density = 2.60 g/cm^3, F.M. = 2.59, Water absorption = 2.20%
Chemical admixture	Superplasticizer	Naphthalene sulfonic acid type
Steel	Round bar	Yield strength = 354 N/mm^2

The specimen discussed in this section is shown in Figure 3. The specimen has a bending crack. The water cement ratio and residual crack width of each specimen are listed in Table 2.

The steel bars were formed from seven steel elements, with the purpose of measuring the macrocell corrosion current using zero resistance ammeters. After the bars were cut into 4.5-cm lengths, lead wires were soldered to both ends of the segments. The neighboring steel elements were connected using epoxy resin with a high insulating capacity. In addition, the reinforcing bars coated with epoxy resin were set in parallel to a specially connected steel bar. The role of this epoxy-coated steel reinforcement was to carry the bending load and produce bending cracks without destroying the specially connected steel bar.

The specimens were cured in a high-humidity environment at 80% RH and 20°C for 28 days. Some specimens were subjected to a bending load to produce a crack at the tension side. Then, the specimens were exposed to an accelerated corrosion environment for 13 weeks. The accelerated corrosion environment consisted of a wet and dry cycle, with wet being exposure to a saltwater shower (NaCl 3.5 wt%) at 90% RH for a 24-h period and dry being exposure to a air at 50% RH for a 60-h period.

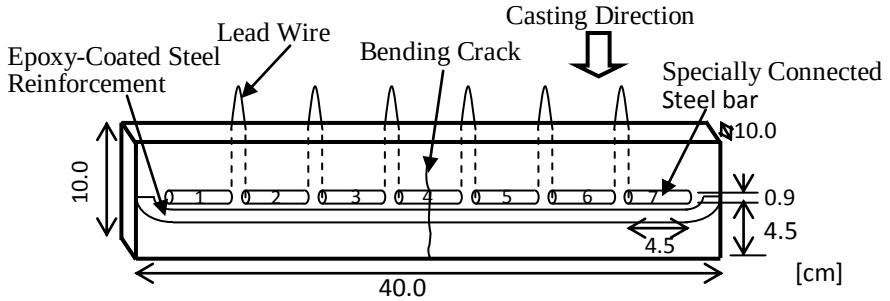

Figure 3. Specimen configuration

Table 2. Experimental cases

W/C (%) \ Residual crack width (mm)	No crack	0.1	0.3	0.7
30			○	
50	○	○	○	○
70			○	

Measurement. The macrocell corrosion current density, potential, polarization resistance, and electrical resistivity of the mortar were measured.

The macrocell corrosion current is the total electric current flowing through all of the adjoining steel elements. For example, the macrocell corrosion current density of steel element No. i shown in Figure 4 is given by Equation 4. The anodic current density is presented as positive, whereas the cathodic current is presented as negative.

$$a_i = \frac{A_{i-1,i} + A_{i+1,i}}{S_i} \tag{4}$$

where a_n = macrocell current density at steel element No. n (μA/cm^2), S_n = surface area of steel element No. n (cm^2), and $A_{n,m}$ = electric current flowing from steel element No. n to No. m (μA).

The potential of the steel element was measured using a saturated copper sulfate electrode for the reference electrode, under the condition of lead wires connected between adjoining steel elements. The polarization resistance of the steel element was determined by the AC impedance using an FRA (frequency response analyzer), as shown in Figure 5. The measurement was carried out using 50 mV and a frequency range of 5000–0.05 Hz. The electrical resistivity of the mortar between adjoining steel elements was measured using a resistance meter, as shown in Figure 6, after disconnecting the lead wire between the steel elements.

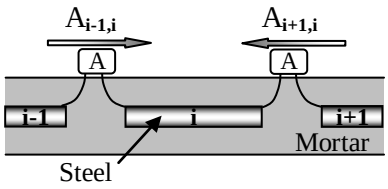

Figure 4. Measurement of macrocell corrosion current

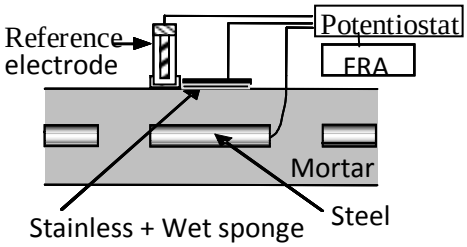

Figure 5. Measurement of polarization resistance

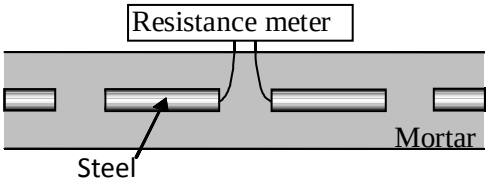

Figure 6. Measurement of electrical resistivity of mortar between adjoining steel elements

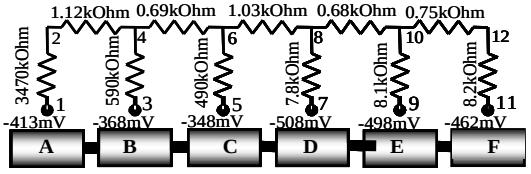

(1) Examples of measured potentials, polarization resistances, and electrical resistivities of mortar

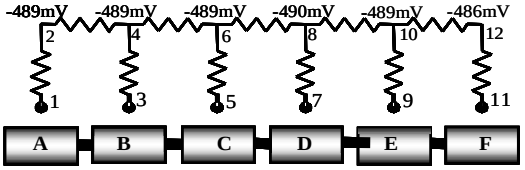

(2) Examples of potentials in concrete, which are medium data to analyse macrocell corrosion current

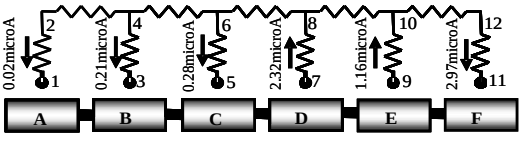

(3) Examples of analyzed macrocell corrosion currents

Figure 7. Example of input and output data in electrical circuit model

Then, the potentials, polarization resistances, and electrical resistivities were substituted in the proposed electric circuit model, and the macrocell corrosion currents were analyzed, as shown in Figure 7.

Comparison between Analyzed and Measured Values. The macrocell corrosion current density distributions are shown in Figures 8 & 9. Figure 8 shows the case with a water cement ratio of 30% and a crack width of 0.3 mm, whereas Figure 9 shows the case with a water cement ratio of 50% and a crack width of 0.3 mm. Based on these figures, both the analysis and measurements confirm that the steel element across the bending crack becomes an anode. In addition, the analyzed and measured values may be equal quantitatively.

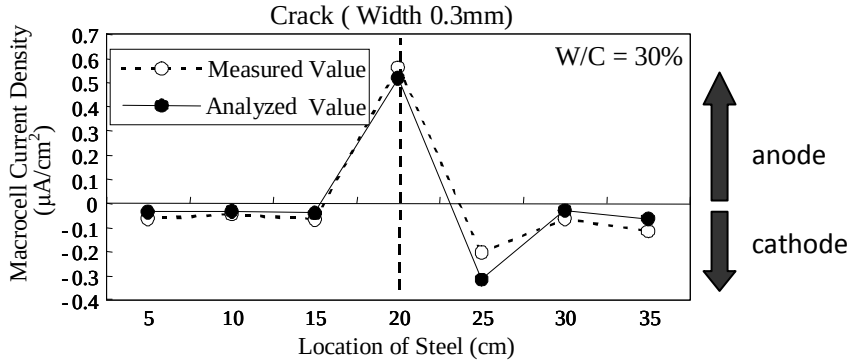

Figure 8. First example of macrocell current density distribution

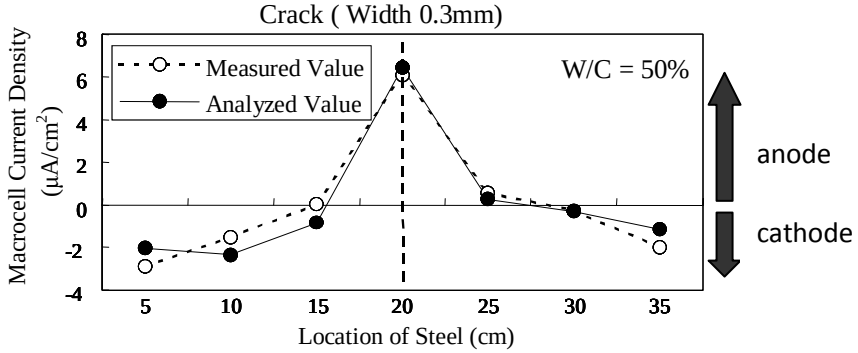

Figure 9. Second example of macrocell current density distribution

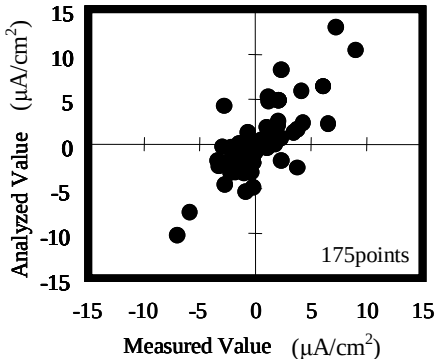

Figure 10. Comparison of all analyzed and measured values of macrocell corrosion current density

The relationship between the analyzed and measured values for all of the specimens is shown in Figure 10. This figure confirms that the analyzed and measured values are approximately equal. Therefore, it becomes clear that the macrocell corrosion current can be estimated using this electric circuit model.

MONITORING FOR EXISTING STRUCTURES

Structures. The monitored structure was a PC T-girdle of a road bridge located along the seashore in Hokuriku. The bridge is 100 m away from the coastline, as shown in Figure 11. The bridge was repaired twice in 1983 and 1988 after its completion in 1972. The monitoring setup is shown in Figure 12. The object to be monitored was a piece of steel that was placed at the bottom of the second girdle from the seashore. Its cover thickness was 50 mm, its surface was painted, and there were no cracks. Also, the chloride ion content near the steel was under the threshold value. The mixture proportion of the concrete is listed in Table 3, and the climate conditions are listed in Table 4.

Figure 11. Complete view of monitored bridge at Hokuriku

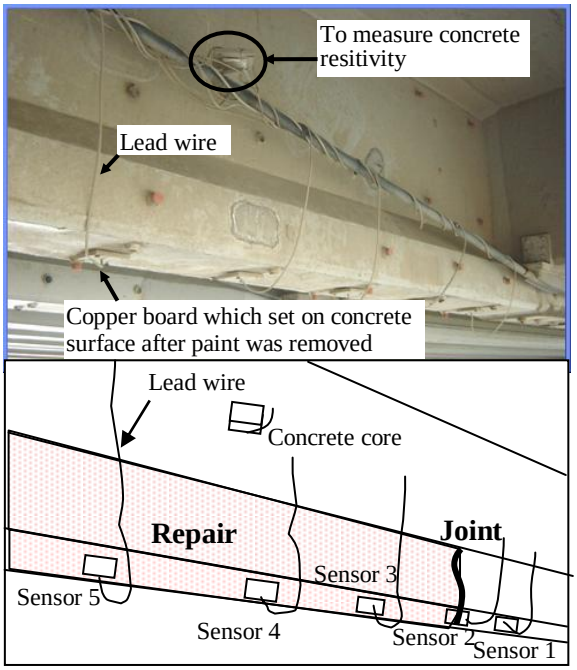

Figure 12. Monitoring setup at bridge

Table 3. Mixture proportion

W/C (%)	Unit quantity (kg/m^3)		
	Water	Cement	Aggregate
39	156	400	1814

Table 4. External environment of structure

Season (Month)		Spring (3,4,5)	Summer (6,7,8)	Autumn (9,10,11)	Winter (12,1,2)
Temperature (°C)	Maximum	27.3	35.6	29.9	18.2
	Minimum	3.7	17.9	9.8	-2.2
Wind velocity (m/s)	Maximum	15.8	16.7	21.1	17.4
	Average	4.0	3.6	3.8	4.6

Measurements for Monitoring. As shown in Figure 12, the bars and the copper boards used to measure the potential and polarization resistance were connected to the AC impedance apparatus by lead wires. Also the core used to measure the electrical resistivity of the concrete was connected to the AC impedance apparatus by lead wire. The input data for the electric circuit model were measured every hour. The monitoring period was from June 2004 to Jan. 2005, excluding in parts of Sep. and Oct. due to the accident to machinery.

Next, some of the values measured at the bridge are shown. The measured potential is shown in Figure 13. The measured polarization resistance is shown in Figure 14. The measured electrical resistivity of the concrete is shown in Figure 15. These figures confirm that the measured values change considerably in winter. This is believed to be because the seasonal wind from the sea is strong in the winter in this area.

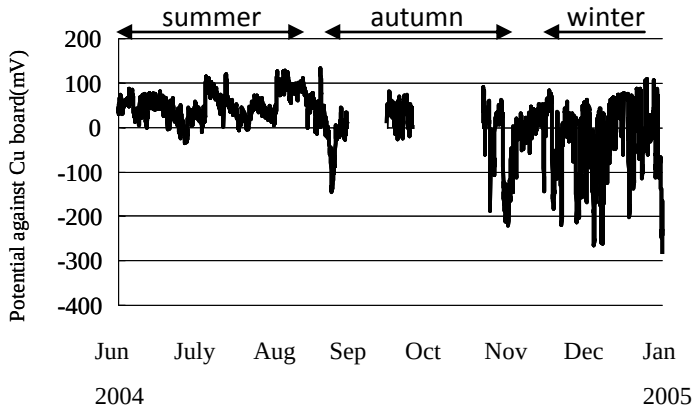

Figure 13. Measured potential at bridge

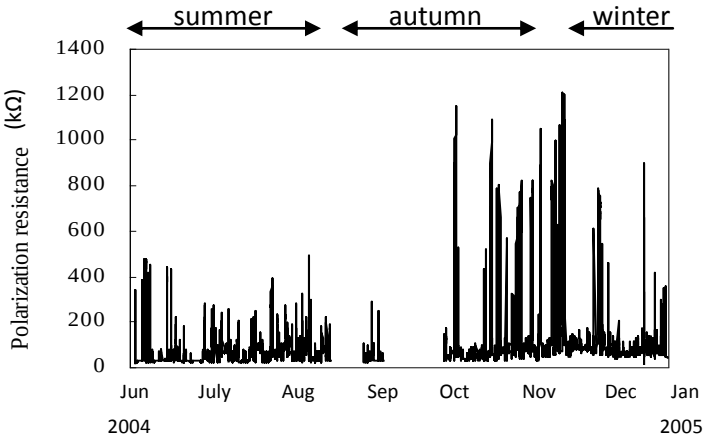

Figure 14. Measured polarization resistance at bridge

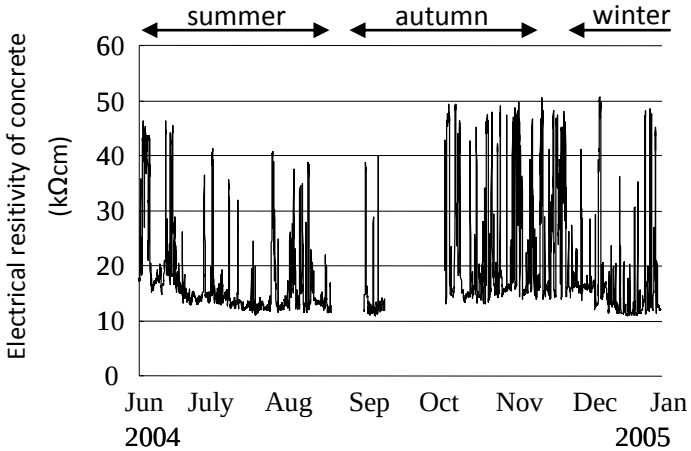

Figure 15. Measured electrical resistivity of concrete at bridge

Analysis. The measured potential, polarization resistance, and electrical resistivity of the concrete were used in the electrical circuit model, and the macrocell corrosion current was analyzed every hour.

Next, an example of the analysis procedure at the bridge is explained. First, the measured potentials, polarization resistances, and electrical resistivities of the concrete are used in the electric circuit model, as shown in Figure 16.

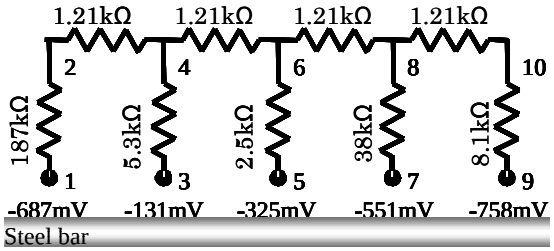

Figure 16. Example of values measured at bridge used in model

Next, Equations 5–9, which correspond to Equation 3, are derived. These have five unknown factors, V_2, V_4, V_6, V_8, and V_{10}, which are the potentials at points 2, 4, 6, 8, and 10 in Figure 16, respectively.

$$\frac{V_1 - V_2}{R_{12}} + \frac{V_4 - V_2}{R_{42}} = 0 \qquad \therefore \frac{-687 - V_2}{187} + \frac{V_4 - V_2}{1.21} = 0 \tag{5}$$

$$\frac{V_2 - V_4}{R_{24}} + \frac{V_3 - V_4}{R_{34}} + \frac{V_6 - V_4}{V_{64}} = 0 \qquad \therefore \frac{V_2 - V_4}{1.21} + \frac{-131 - V_4}{5.3} + \frac{V_6 - V_4}{1.21} = 0 \tag{6}$$

$$\frac{V_4 - V_6}{R_{46}} + \frac{V_5 - V_6}{R_{56}} + \frac{V_8 - V_6}{R_{86}} = 0 \qquad \therefore \frac{V_4 - V_6}{1.21} + \frac{-325 - V_6}{2.5} - \frac{V_8 - V_6}{1.21} = 0 \tag{7}$$

$$\frac{V_6 - V_8}{R_{68}} + \frac{V_7 - V_8}{R_{78}} + \frac{V_{10} - V_8}{R_{108}} = 0 \qquad \therefore \frac{V_6 - V_8}{1.21} + \frac{-551 - V_8}{38} + \frac{V_{10} - V_8}{1.21} = 0 \tag{8}$$

$$\frac{V_8 - V_{10}}{R_{810}} + \frac{V_9 - V_{10}}{R_{910}} = 0 \qquad \therefore \frac{V_8 - V_{10}}{1.21} + \frac{-758 - V_{10}}{8.1} = 0 \tag{9}$$

Equations 5–9 are independent. Therefore, the potentials in the concrete can be calculated, as shown in Figure 17, by solving the simultaneous equations.

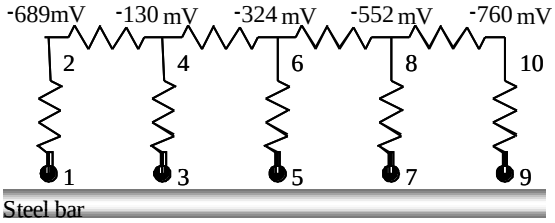

Figure 17. Examples of potentials in concrete of bridge, which are medium analysis values

Finally, the potential difference between adjacent points is divided by the resistance using Equation 10, and the value of the macrocell corrosion current that flows between the points is calculated as shown in Figure 18.

$$
\left.
\begin{aligned}
I_{12} &= \frac{V_1 - V_2}{R_{12}} = \frac{(-687) - (-689)}{187} = 0.01\,\mu A \\
I_{34} &= \frac{V_3 - V_4}{R_{34}} = \frac{(-131) - (-130)}{5.3} = -0.17\,\mu A \\
I_{56} &= \frac{V_5 - V_6}{R_{56}} = \frac{(-325) - (-324)}{2.5} = -0.05\,\mu A \\
I_{78} &= \frac{V_7 - V_8}{R_{78}} = \frac{(-551) - (-552)}{38} = 0.02\,\mu A \\
I_{910} &= \frac{V_9 - V_{10}}{R_{910}} = \frac{(-758) - (-760)}{8.1} = 0.19\,\mu A
\end{aligned}
\right\} \quad (10)
$$

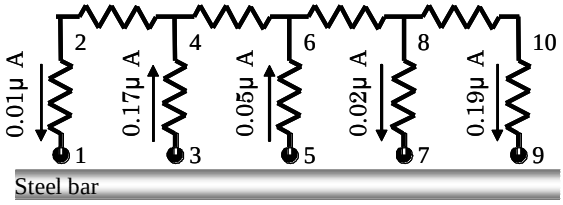

Figure 18. Examples of analyzed macrocell corrosion currents at bridge

Herein, the steel is the anode when the macrocell corrosion current is flowing out from the steel surface. On the other hand, the steel is the cathode when the macrocell corrosion current is flowing into the steel surface. Therefore, in Figure 18, the steels at points 3 and 5 are anodes and the steels at points 1, 7, and 9 are cathodes.

Monitoring Results. The macrocell corrosion rate monitoring results are shown in Figure 19. This figure confirms that the corrosion rate changes per hour during continuous monitoring. In addition, the macrocell corrosion rate at a bridge with a repair was low.

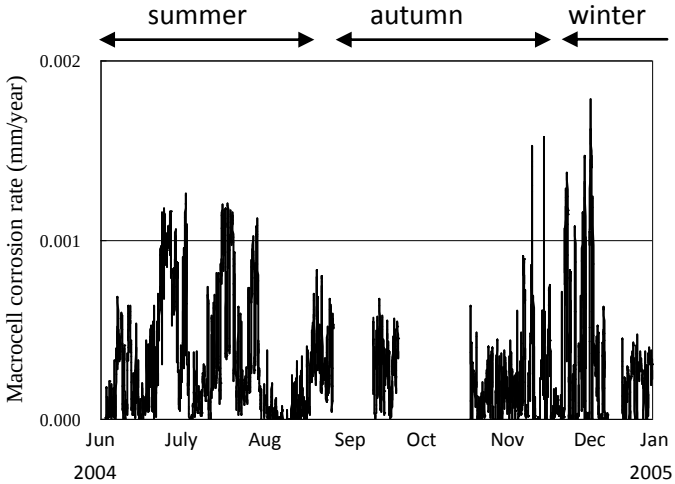

Figure 19. Monitored macrocell corrosion rate at bridge

Relationship of Corrosion Rate. In Figure 20, the average macrocell corrosion rate for a day is compared to the macrocell corrosion rate measured at an arbitrary time. According to

this figure, the macrocell corrosion rate measured at 10 a.m., which was the time when the average daily temperature was recorded, is almost equal to the average for that day. On the other hand, the macrocell corrosion rate at 5 a.m., which was the time when the minimum temperature for that day was recorded, is different from the average for that day.

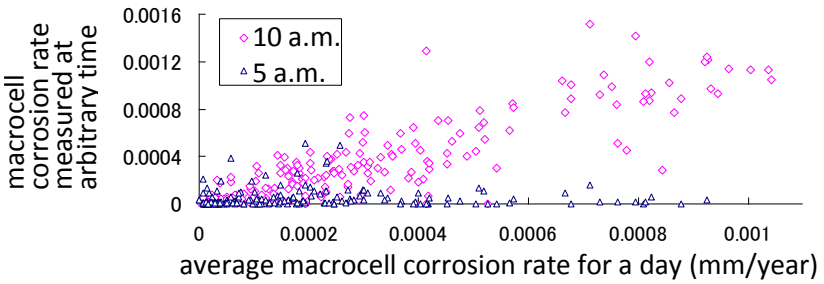

Figure 20. Relationship between macrocell corrosion rate at arbitrary time and average macrocell corrosion rate for day

CONCLUSIONS

The conclusions are as follows:

1) The macrocell corrosion rate could be monitored at an existing reinforced concrete structure.
2) An electric circuit model that simulated a macrocell in the reinforced concrete was proposed. The input data for this model included the potentials of the bar, polarization resistances of the bar, and electrical resistivities of the concrete, whereas the output data were the macrocell corrosion currents.
3) The validity of this analysis method was confirmed by experiments using a mortar specimen with a crack and an existing reinforced concrete structure with a repair. As a result of the specimen experiment, the analyzed and measured values of the macrocell anode locations and corrosion rates were found to be quantitatively equal. In addition, the macrocell corrosion rate could be monitored at the existing reinforced concrete structure.
4) The corrosion rate measured at 10 a.m. was found to be the average for the day. Therefore, it is considered that the corrosion condition of a structure can be quantitatively estimated by measuring the corrosion rate at 10 a.m.

ACKNOWLEDGMENT

The author appreciates the advice given by Prof. Otsuki at the Tokyo Institute of Technology, the support of the Kanazawa branch of Japan Highway, and the cooperation of Dr. Hiraishi.

REFERENCES

Miyazato, S. and Otsuki, N. (2010). “Steel Corrosion Induced by Chloride or Carbonation in Mortar with Bending Cracks or Joints.” *Journal of Advanced Concrete Technology*, 8 (2) 135-144

Otsuki, N., Miyazato, S., Diola N. B. & Suzuki, H. (2000). “Influence of Bending Crack and Water cement ratio on Chloride Induced Corrosion of Main Reinforcing Bars and Stirrups,” *ACI Materials Journal*, 97 (4) 454–464